Part III:

Applications

7

Experimental prototype

7.1 Introduction

This chapter presents an experimental proof-of-concept of a smart under-deck cable-stayed footbridge. Specifically, this section describes the design, construction, and testing of a 6-meter-span prototype, which reproduces the structural scheme represented in Figure 1.1.

The main objective of this work is to experimentally evaluate the applicability of the system in a real structure. In particular, the prototype allows for verifying the correct integration of the technological system into the structure and understanding the real technological limitations of the instrumentation.

Furthermore, the construction of the prototype is also useful for experimentally validating the analytical formulations and numerical models describing the structural behavior of under-deck cable-stayed structures. Finally, although the design of the smart system has been carried out to improve the structural behavior from a static perspective, the dynamic experimental response is also investigated.

The work described in this chapter has been illustrated in a short video which can be accessed online [83].

7.2 Design and construction

7.2.1 Geometry, materials and structural verifications

The experimental prototype is shown in Figure 7.1a. It has a length of 6 meters and a total width (B) of 0.77 meters. The rise (f) is 0.80 meters when the actuator is in its initial position (before elongation). All the elements are schematically represented in Figures 7.1b and 7.1c.

(a) Picture and identification of the main elements.

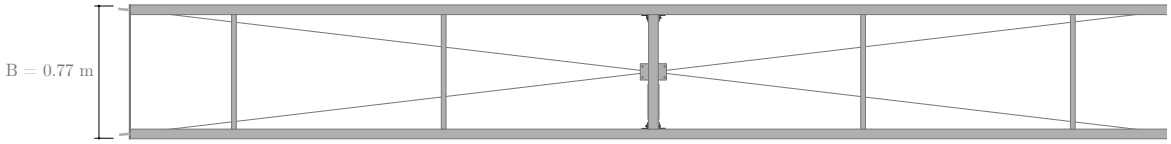

(b) Plan view.

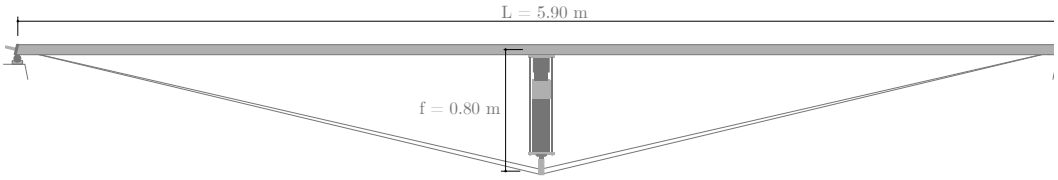

(c) Elevation.

Figure 7.1: Experimental prototype.

The deck is made up of two simply supported steel beams, with a square hollow cross-section of 60 x 60 x 2 mm and an effective span (L) of 5.9 meters. On top of these beams, ten glass panels with dimensions of 600 x 770 x 12 mm are placed to provide a flat surface for walking. These glass panels have no structural purpose. At midspan, a transverse steel beam (60 x 30 x 3 mm) is connected to the longitudinal beams with hinged connections. The linear actuator is located in the middle of this transversal beam, with pinned connections at both ends to avoid any bending in this element. Consequently, it is only capable of perfectly counteracting loads applied in the centerline of the footbridge. Two actuators should be placed (one for each longitudinal beam) in a full-scale structure to extend its effectiveness also to eccentric loads.

To increase the torsional stability, four additional transverse steel beams are distributed along the span to connect the two longitudinal beams. These beams are fixed at both ends and have a rectangular hollow cross-section of 30 x 60 x 3 mm. No specific material tests were performed and the steel manufacturer's yield stress ($f_{sy} = 275$ MPa) was assumed.

The under-deck cable-stayed system, provided by Aciarium, consists of two 7x19 stainless steel cables, each with a diameter of 6 mm. These are very flexible cables with relatively low resistance (breaking load of 21.07 kN/cable). Each cable connects the opposite ends of the two beams, passing through a deviator located at the bottom end of the actuator, specifically made for this prototype (Figure 7.2a). The deviator is formed by two pieces which can rotate independently around the vertical axis to accommodate to the angle formed by the cables.

The connection of the cables to the beam has been designed to transfer the tension load of the cable to the beam as a pure compression force. For this, a hole has been drilled in the underside of the beam, next to the support. The end of the beam has been cut at the same angle as the one formed by the cables to the beam (13.2°) and a steel plate with two holes has been placed at the end, acting as a bracing element. External threads are connected to both ends of the cables. The cables pass through the beam and the steel plate, to finally connect to the beam with a swiveled nut (Figure 7.2b). This nut allows the cable to freely rotate about its support when the length of the actuator varies.

Theoretically, this type of connection guarantees that the tension force is always transmitted as a pure compression force to the beam. Consequently, bucking of the longitudinal steel beams has to be verified. Based on the worst-case scenario of the prototype (i.e. the actuator fully compensating the weight of ten people), the maximum compression force in the beam is $N = 6.6$ kN. The critical buckling load, obtained according to Euler's formula, is $N_E = (\pi^2 \cdot E \cdot I)/L^2 = 15.5$ kN, so buckling in the beams is largely fulfilled.

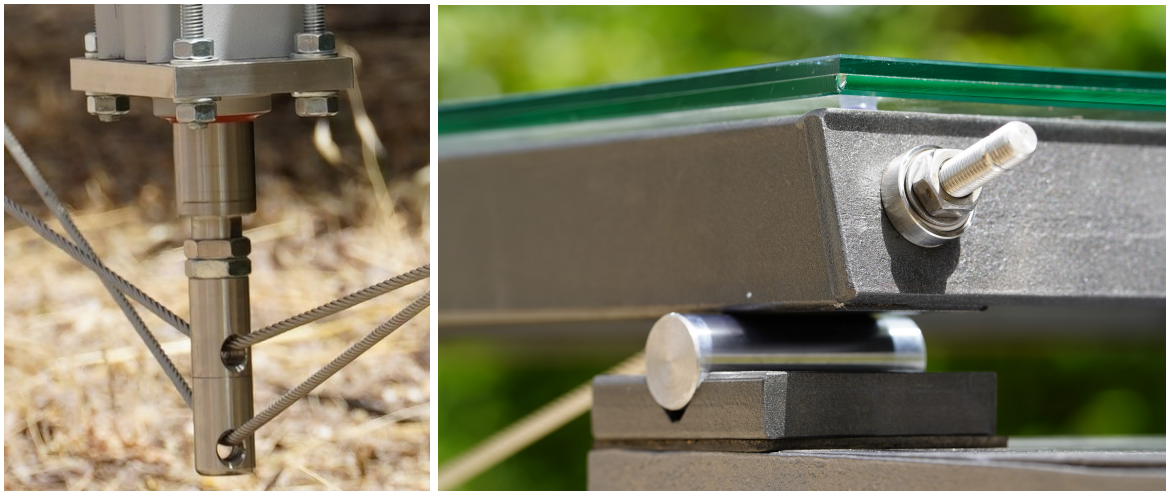

(a) Deviator at bottom end of the actuator

(b) Connection of the cables to the longitudinal beam.

Figure 7.2: Details of the prototype.

Overall, the prototype has been designed to largely fulfill the Ultimate Limit State when loaded with ten people of average weight in two extreme conditions: when the actuator does not work (worst condition for the beam) and when the actuator compensates all live load at midspan (worst condition for the cable-stayed system). A minimum safety factor of 2.0 has been adopted for all global and local verifications.

According to Eurocode 3 [22], ULS requirements in the beam include the verification of $\sigma_{Ed} \leq f_{sy}/\gamma_{M0}$, being σ_{Ed} the design stress value of the beam, $f_{sy} = 275$ MPa the yield strength of the material and $\gamma_{M0} = 1.0$ the partial factor for the resistance of the cross-section. These verifications are performed using the section forces obtained from both the analytical and numerical methods described in Section 7.3.2. The Serviceability Limit State requirements for the beam are not fulfilled, as the primary objective of the prototype is to achieve visible displacements.

The under-deck stays have been designed according to Part 1–11 of Eurocode 3 [22], which indicate the following verifications: $F_{ULS} \leq F_{uk}/1.5$ and $F_{SLS} \leq 0.45 \cdot F_{uk}$. F_{ULS} and F_{SLS} are, respectively, the design values of the axial forces at ULS and SLS and F_{uk} is the characteristic value of the breaking strength, as provided by the manufacturer (21.07 kN).

7.2.2 Smart system

The smart system consists of three main elements: displacement sensor, control system, and actuator. The sensor is in charge of measuring deck deflections at midspan. This information is processed by a Programmable Logic Controller (PLC), which communicates with the linear actuator if a movement has to be performed. These parts work together as a closed-loop system. The loop is continually repeated every 10 ms, guaranteeing constant feedback. All the devices have been supplied by the company FESTO, so they have been selected from their product catalog. Next, each part of the smart system is individually analyzed.

The selected displacement sensor consists of a position transmitter (magnetic sensor) and a 100 mm-stroke pneumatic cylinder, as shown in Figure 7.3a. The fixed part of the pneumatic cylinder rests on the ground, whereas an inner piston is attached to the bottom face of the deck. When the deck deflects, the piston is introduced into the cylinder a distance equal to this deflection. The position transmitter (SDAT) is used to obtain the position of the piston (4-20 mA analog signal output). This signal is sent to the control system, allowing constant monitoring of the deflection. It is noted that for real-scale applications, it is suggested to use a non contact sensor as a laser sensor. This kind of instrumentation was also tested with the prototype, achieving almost identical results. Also, several sensors should be employed.

The actuation is achieved through an electric linear actuator. Although the cost of electric actuators is generally higher than, for example, pneumatic or hydraulic cylinders, they present a series of advantages such as high precision and low maintenance. For the prototype, a Festo ESBF series linear actuator with a maximum cylinder force of 12 kN and a stroke of 100 mm was used (Figure 7.3b). The working mechanism is of ball-screw type, guaranteeing a high accuracy of displacements. The movement can reach a maximum speed of 0.21 m/s and a maximum acceleration of 5 m/s^2. The actuator has a nominal energy consumption of 690 Watts.

(a) Displacement sensor. **(b)** Linear actuator.

Figure 7.3: Main elements of the smart system.

A PLC is necessary to interpret the data collected by the sensor and to provide instructions to the electric actuator. Communication between the PLC and the rest of the devices is carried out using the Ethercat communication protocol. A master-slave communication model is used: the communication between all devices is governed by the PLC, which can access the parameter configuration of the slaves. The selected PLC is from the CPX-E Festo family, as it allows for this type of communication and includes an analog input module, which is necessary to process the data provided by the sensor. As a graphical summary, the complete hardware configuration of the smart system is shown in Figure 7.4.

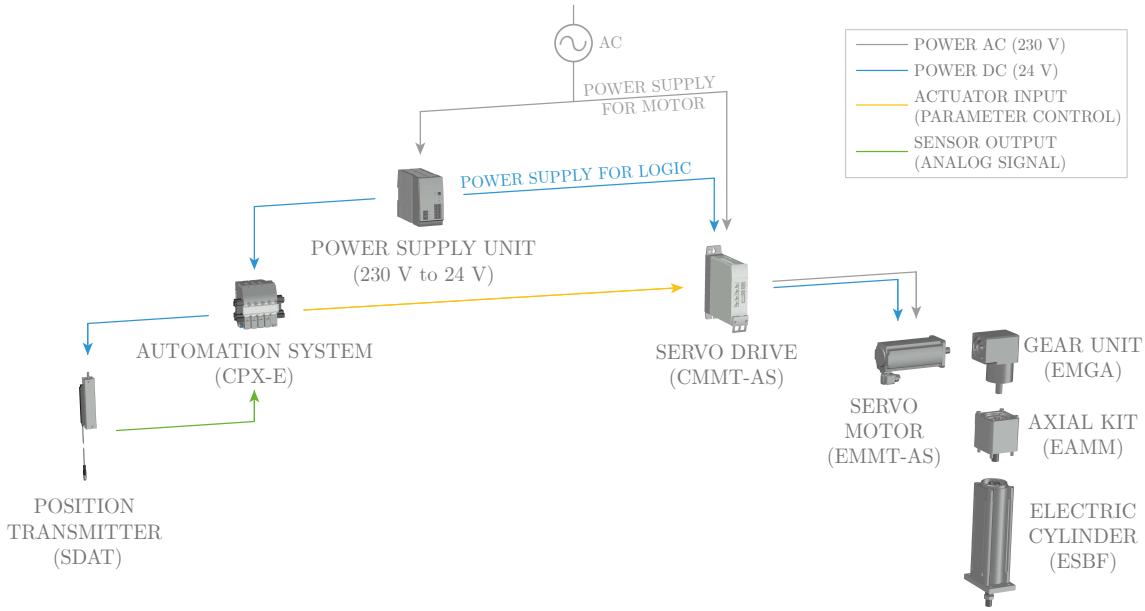

Figure 7.4: Smart system hardware.

7.2.3 Control strategy

The control strategy is designed with the goal of identifying the optimum elongation of the actuator at each moment, based on the displacement read by the sensor. The control strategy adopted in the prototype consists of a simple ON/OFF closed-loop control system. The input of the system is the midspan deflection of the deck: when it exceeds a certain value (threshold), a movement instruction is sent to the actuator. The output of the system is the instruction to the actuator.

Due to delays in the response of the system, it is not possible to have a perfect and real-time compensation of the displacement, as the elongation of the actuator would oscillate constantly around the limiting value. To solve this issue, two displacement thresholds have been established. When the displacement is lower than the bottom displacement threshold, the actuator elongates. In contrast, when the displacement is greater than the top displacement threshold, the actuator contracts. If the displacement is within both thresholds, the actuator does not move. In summary, the control algorithm is defined as a semi-active ON/OFF control law, in which the minimization of the deflection at midspan is set as the objective function.

To evaluate the performance of the control system, the stability of the response has been chosen as the primary criterion. It has been detected that an adequate gap between the thresholds, depending on the magnitude of the acting load, provides a stable response. It is worth mentioning that the proximity of the actuator and the sensor in the control system configuration (collocated control approach) allows for improved control performance and stability. Another factor that could influence the stability of the system is signal noise. Consequently, a filter has been introduced to detect unrealistic values in the sensor signal. When such values are detected, the filter forces the sensor signal to zero, preventing unnecessary drastic adjustments of the actuator.

The system has been verified to be robust under normal use conditions, but unusual scenarios (e.g., several people jumping) can affect the performance of the system, as the actuator continues to oscillate for a long period. This aspect has not been considered in the tested prototype and should be improved in future developments.

The existence of two thresholds in the system leads to partial observability, since the actuator can have the same elongation for different configurations of live load and displacement. As a result, it is difficult to determine the state of the system solely on the basis of the actuator's position. Although decreasing the gap between these thresholds

can help reduce this level of indeterminacy, such reduction can negatively impact the system stability, so it is important to find a good balance between both aspects. For the current implementation of the system, the established parameters are sufficient to ensure a proper operation.

The command given to the actuator to execute or not a movement is updated every 10 ms, which is the time it takes the system to complete a loop (bus cycle), conditioning the delay of the response. To minimize any additional delays, the actuator remains continuously on, assuring that once the command to move is given, it is performed without any additional time retards. However, this approach leads to increased energy consumption. Therefore, the system performance was also evaluated with the actuator inactive until the signal exceeded the specified thresholds. Unfortunately, this strategy resulted in poor performance, so the former approach (actuator always on) was selected.

Several measures are taken to avoid system failures. Regarding the sensor, the previously mentioned filter allows to detect and ignore unrealistic values in the signal. The linear actuator is instantly self-locked in its current position if there is a power shortage, so the structure starts to work as a conventional under-deck cable-stayed footbridge. The prototype has been designed to amply withstand this situation.

In this ON/OFF control strategy, the speed and acceleration of the actuation are constant values, set as input values of the system. This leads to several limitations of the response, which can be improved by using more sophisticated control strategies, such as Proportional-Integral (PI) and Proportional–Integral–Derivative (PID) Controls. The implementation of these strategies would also allow overcoming the limitations previously described.

The programming and parameterization of the devices were done using the software CODESYS, an integrated development environment for PLC applications, together with Festo's own program (Festo Automation Suite). In order to easily visualize some of the main parameters of the system, a real-time interface was developed, as shown in Figure 7.5.

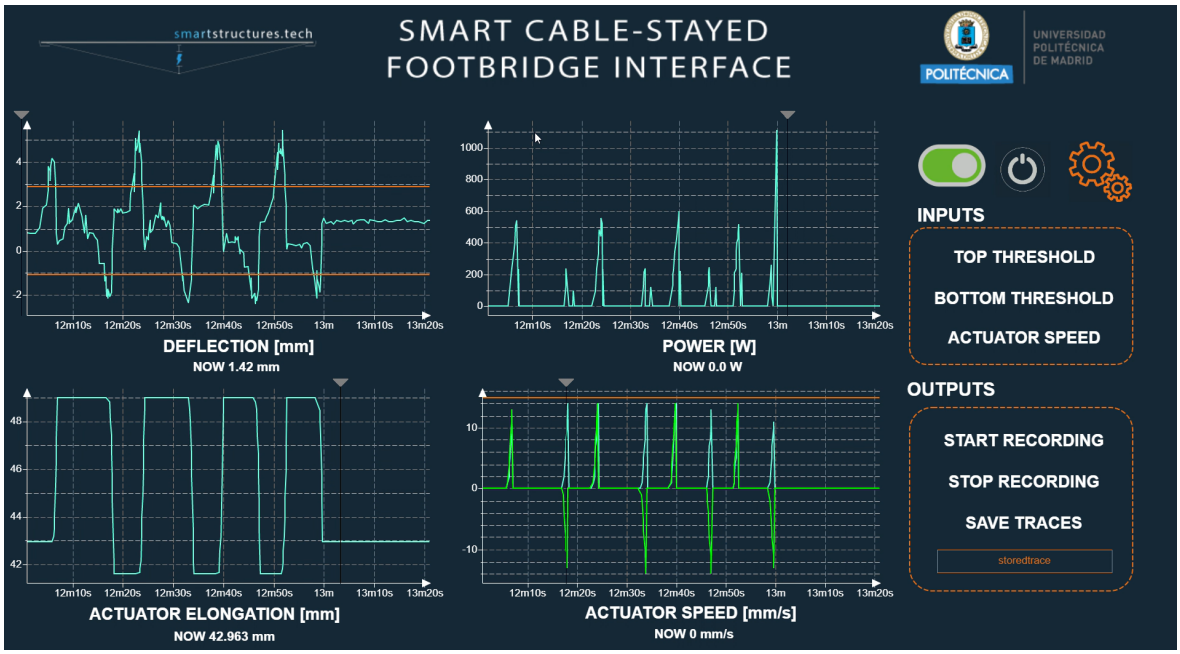

Figure 7.5: Smart cable-stayed footbridge interface.

This interface allows to provide immediate feedback on a variety of variables such as the displacement of the deck at midspan (top-left corner), power consumed by the actuator (top-right corner), actuator elongation (bottom-left) and actuator speed (bottom-right). All of these data can be visualized in real-time or stored for further processing. Other parameters, such as the speed and the acceleration of the actuator, can be controlled from the same interface.

7.3 Experimental testing under static and quasi-static loads

7.3.1 Testing procedure

The first step in the experimental campaign consisted of comparing the results obtained from different tests performed under different static load conditions with the expected results according to analytical and numerical models.

The displacement at the deck midspan, as well as the elongation of the actuator, were outputs provided by the smart system. In these static tests, the smart system is controlled manually. In addition, a load cell was installed between the actuator and the transversal beam located at midspan. This load cell allowed to quantify the portion of the vertical load going through the actuator and, therefore, resisted by the cable-stayed system. The remaining part

of the applied load is resisted directly by the deck, working in bending.

The static tests consisted of two steps: i) to elongate the actuator to achieve a deflection equal to zero at midspan for the permanent loads, ii) to gradually place 4 sand bags (of 20 kg each) at midspan, representing the live load. This second step was performed without smart behavior (i.e. the actuator does not work) and with smart behavior (i.e. the actuator elongates to keep the displacement equal to zero at midspan also when bags are added).

7.3.2 Analytical and numerical models

The analytical model used to quantify the internal load distribution between the deck and the cable-stayed system for live loads has been described in Chapter 4. For a conventional under-deck cable-stayed structure, when loaded with a point load Q, the axial force in the midspan strut is $R_Q = Q \cdot \xi_Q$. The value of ξ_Q can be obtained with Equation 4.10. The deflection at midspan also depends on ξ_Q and is obtained as:

$$v_z = \frac{Q \cdot L^3 \cdot (1 - \xi)}{48 \cdot E_s \cdot I} \qquad [\text{mm}] \tag{7.1}$$

where L is the span of the beam and E_s and I are, respectively, the Young Modulus and the inertia of the longitudinal beams.

When the smart system is working, the axial force in the strut when loaded with a point load Q takes a value of $R_Q = Q$ (i.e., ξ takes a fictitious value equal to 1, meaning that the totality of the load is resisted directly by the cable-stayed system). In this case the deflection at midspan is zero.

In addition to the analytical formulation, a numerical model was also developed. As shown in Figure 7.6, the prototype was modeled in SOFiSTiK, a finite element software for structural analysis. This model strives to replicate the structural behavior of the prototype as closely as possible.

The two longitudinal beams, the five transversal beams and the actuator are modeled as beam elements. Truss elements, which only carry axial loads, have been used for the under-deck cable-stayed system. These elements are connected with hinges to the longitudinal beams. The longitudinal beams are experimentally supported by thin rubber layers, which are numerically simulated by springs located at the four corners with specific stiffness in the three principal directions.

Permanent loads are estimated using the real cross-section geometry and unit weight, while pedestrian loads are applied directly to the longitudinal beams. The elongation of the actuator is simulated by introducing a strain in the strut in its axial direction. A linear analysis, including both geometrical and material linearity, is considered using SOFiSTiK's beam element formulation, that accounts for shear deformation and hinge behavior.

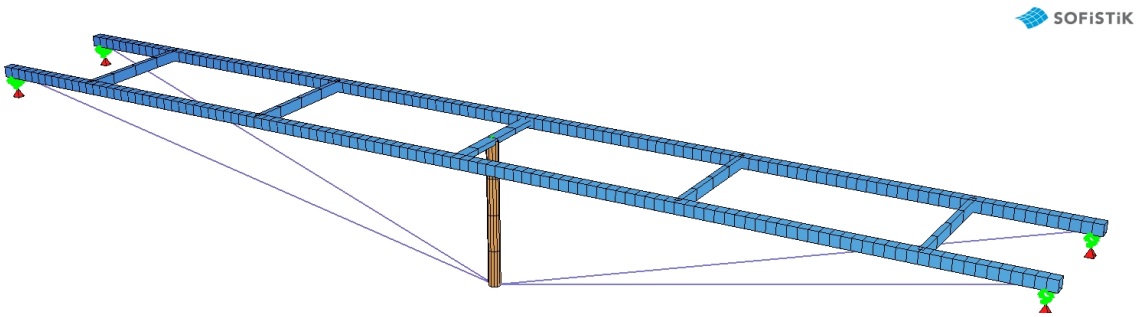

Figure 7.6: 3-Dimensional numerical model of the prototype.

The geometry and cross-sections adopted in the analytical and numerical approaches are the same as in the experimental prototype. The Young Modulus of the beams and the cables were iterated until the results were as close as possible to the experimental ones. This calibration led to a Young Modulus $E_s = 200$ GPa for the beam and $E'_s = 87$ GPa for the cables. These values are consistent with the theoretical Young Modulus of the materials, which are $E_s = 210$ GPa for steel elements and $E'_s = 100$ GPa for the selected cables, as specified by the manufacturer. Despite the slight differences, the ratio E_S/E'_s is similar for both experimental and theoretical values (2.3 and 2.1, respectively), confirming the reliability of the obtained Young Modulus.

7.3.3 Comparison between experimental, analytical and numerical results

Figure 7.7 plots the comparison of experimental, analytical and numerical values of the axial force in the strut for different applied live loads, considering conventional and smart structural behavior.

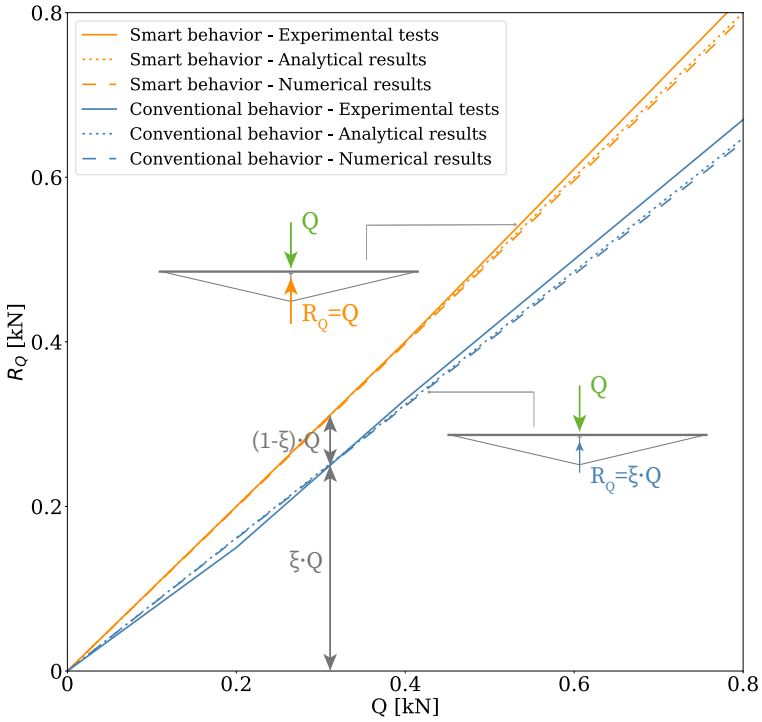

Figure 7.7: Comparison of experimental, analytical and numerical values of the axial force in the strut (R_Q) for different applied live loads, considering conventional and smart structural behavior.

The tests performed with smart behavior show a trend line with an angle of almost 45° with the horizontal, which means that the entire live load goes directly to the cable-stayed system ($R_Q = Q$). Small differences in the experimental test measures are due to inaccuracies of the load cell (insufficient precision). In contrast, the tests carried out with a conventional structural behavior (no smart system activated) show that the load resisted by the cable-stayed system is reduced, as the beams and the cables work together to withstand the live load. As mentioned above, the contribution of the cable is proportional to the factor ξ, in this case around 0.81 (which means that 81% of Q is resisted by the cable-stayed system).

As a main finding, the differences between the experimental tests and the numerical and analytical values oscillate between 4-8%. These differences can be considered sufficiently small, showing a good performance of the prototype and a good analogy between the theoretical models and the experimental prototype.

Although not graphically shown in the work, the experimental results of the deflections of the deck (for conventional structural behavior) and the elongation of the actuator (for smart structural behavior) also showed a good fit with the analytical and numerical models.

7.3.4 Influence of the prestressing

As already mentioned, the internal force distribution under permanent loads depends on the initial value of the prestress force. Analytically, this is expressed with the adimensional parameter ρ, which is the portion of permanent loads compensated by the prestressing system [4]. In the previous tests, ρ was set to 1, meaning that initially there are no deflections at midspan.

As shown in Chapter 4, specifically in Equation 4.1, the behavior in the permanent state depends on ρ. However, since ρ does not interfere in the analytical formulation of the live load, the structural behavior under live loads does not depend on the initial prestressing of the tendons. In order to experimentally prove this statement, some additional tests were performed, following the same procedure as above. Specifically, three tests were done for the three following initial configurations of the cable-stayed system:

- Test 1. The initial prestress force is set to achieve $\rho = 1$ (no deflection at midspan). The permanent load is calculated from the dimensions of the prototype ($g_1 = 0.33\,\mathrm{kN/m}$).
- Test 2. Two sand bags of permanent load are added ($g_2 = g_1 + 40\,\mathrm{kg}$). Consequently, the initial prestress force is increased ($\rho \approx 1.05$) to obtain a deflection equal to zero at midspan (without changing the elongation of the actuator).
- Test 3. Four sand bags of permanent load ($g_3 = g_1 + 80\,\mathrm{kg}$) are added, but the initial prestress force is not varied ($\rho = 1$). The actuator elongates 9.2 mm to obtain a deflection equal to zero at midspan (i.e., the rise is increased).

Figure 7.8 plots, on the vertical axis, the axial force in the strut (R_Q) versus different values of the live load (horizontal axis). Tests 1 and 2 provided almost identical results, proving that if the geometry is the same, the variation of other parameters (ρ and g) has no effect on withstanding the live load. In contrast, Test 3 sheds light on the effect of increasing the value of f. Since this parameter affects the formulation of ξ and consequently also R_Q, by increasing f, the efficiency of the tensioning system is also enlarged. Thus, the dotted trend line plotted in Figure 7.8 is closer to 45° degrees for test 3 than for tests 1 and 2.

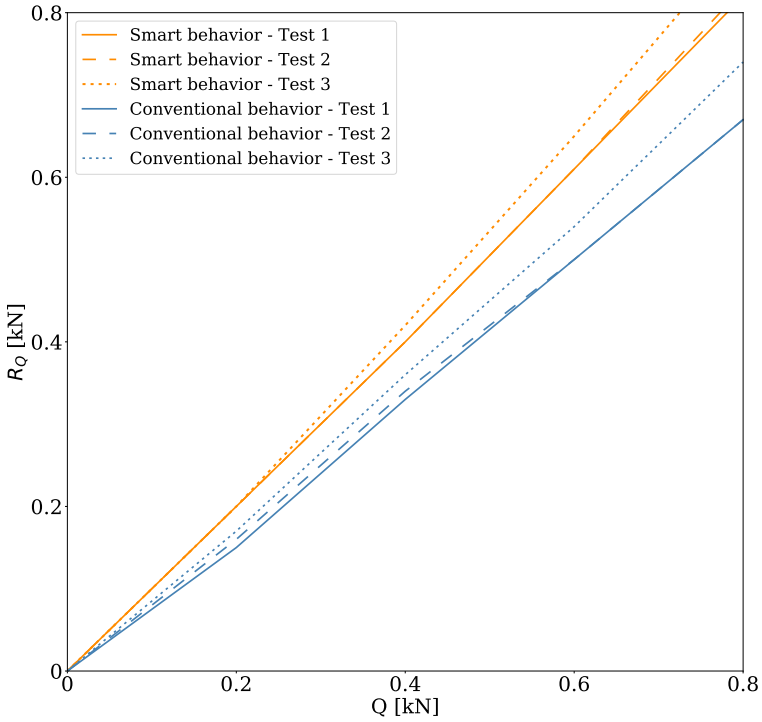

Figure 7.8: Test results. Axial force in the strut for the three tests with different initial configurations.

7.3.5 Performance of the smart system under quasi-static loads

The response of the prototype under quasi-static loads has been investigated with one single pedestrian, two pedestrians and a flow of pedestrians crossing the footbridge. The main parameter to evaluate the efficiency of the smart system is the displacement at midspan. In fact, the performance of the smart system is directly related to the reduction of the displacement respect to the conventional system (i.e., without control).

The displacement in the deck caused by one or several pedestrians is composed by two parts: a static displacement and a dynamic displacement (oscillations around the static displacement). The first depends on the magnitude and position of the load. The second depends on the dynamic characteristics of the load and the structure (see Section 7.4). For each test, two displacement curves are plotted: a dashed curve, representing the actual values measured by the sensor (static plus dynamic displacement) and a solid curve, which only represents the static displacement. This section focuses on the latter, while the dynamic behavior is illustrated in Section 7.4.

The efficiency of the control depends on several parameters, such as the sensor displacement thresholds (described in Section 7.2.3) and the maximum speed and acceleration of the actuator. The response is also highly dependent on the magnitude and speed of the load (i.e., the number of people and their walking speed).

Figure 7.9 plots the experimental displacements obtained at midspan for one person walking at a typical walking speed (approximately 1.0 m/s, taking 6 seconds to cross the footbridge) versus the time (horizontal axis). The tests were performed in three different scenarios: i) simply-supported footbridge (prototype with neither cable-stayed system nor control), ii) conventional under-deck cable-stayed footbridge (prototype with cable-stayed system, but with no control) and iii) smart under-deck cable-stayed footbridge (prototype with cable-stayed system and with an ON/OFF control strategy).

In the first test scenario (the prototype without cable-stayed system), a maximum static deflection of around 30 mm (downwards) is obtained. In this case, due to the low stiffness of the deck, the oscillations around the static displacement reach an amplitude of 32 mm. In addition, once the pedestrian leaves the footbridge (after 6 seconds), the oscillations are slowly damped. This aspect will be further detailed in Section 7.4.

In the second test scenario (conventional under-deck cable-stayed structure), the maximum static deflection is 7.5 mm. Thus, a reduction of 75% can be achieved with respect to the first structural configuration, proving that the use of a cable-stayed system alone is an effective way of reducing deflections also for live loads. In this case, the oscillations of the dynamic component of the deflections are significantly reduced.

Finally, the last test scenario is performed with the smart system. When the displacement exceeds the bottom threshold (set to -1 mm), the actuation is triggered. The actuator starts to elongate as the load continues to move towards midspan. Due to delays in the response, together with the fact that the load is starting to move away from the sensor position, the displacement is overcompensated (higher than zero) and the deck experiments upward displacements. For this reason, there is a top threshold (set to +1 mm) which activates the contraction of the actuator. The maximum displacement (in absolute value) is reduced to one third respect to the second scenario.

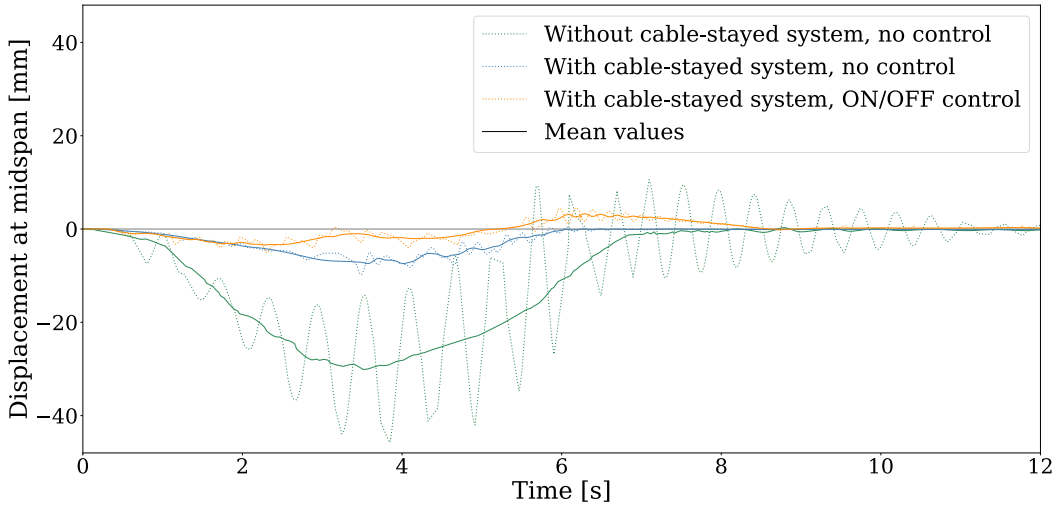

(a) Displacement vs. time for the three test scenarios.

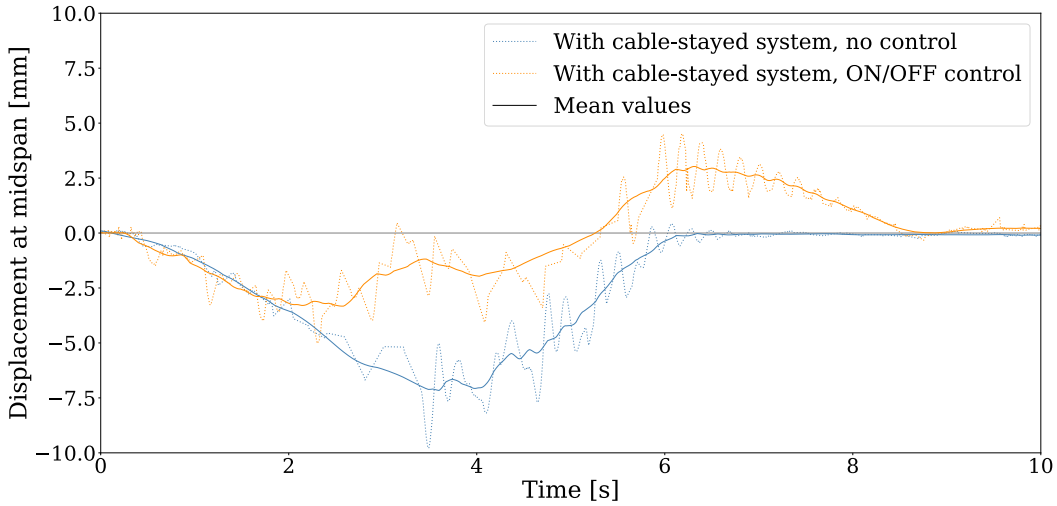

(b) Zoom of displacements vs. time for the test scenarios with cable-stayed system.

Figure 7.9: Experimental values of the displacements at midspan vs. time, for one pedestrian walking at 1.0 m/s.

The results of a similar study are shown in Figure 7.10. In this case, two people crossed the footbridge at a lower speed (0.5 m/s, taking 12 seconds to cross the footbridge). This lower speed allows to increase the efficiency of the smart system despite having increased the load. The displacements at midspan versus the time are shown for two test scenarios: i) the structure without control (acting as a conventional under-deck cable-stayed footbridge) and ii) the structure with smart control (ON/OFF control).

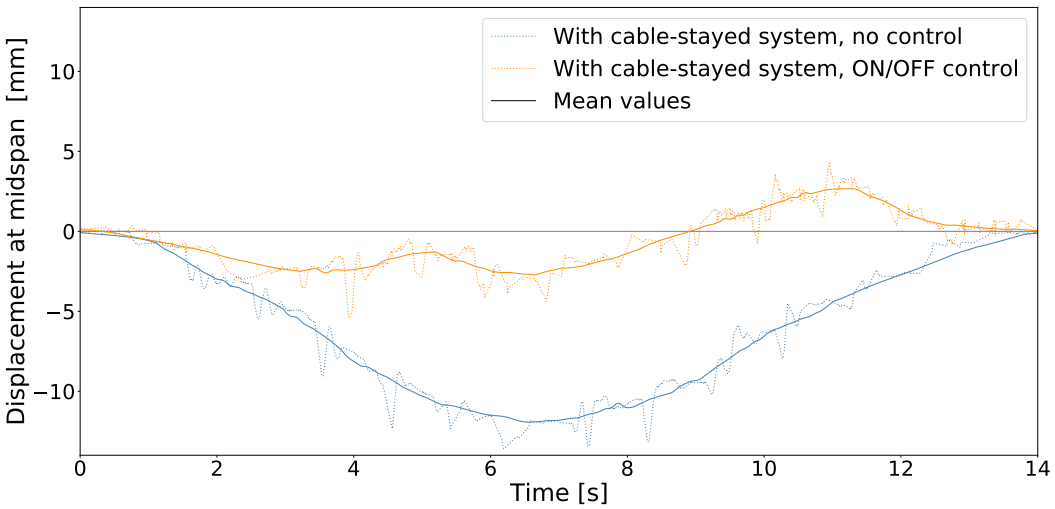

Figure 7.10: Experimental displacements at midspan vs. time, for two pedestrians walking at 0.5 m/s.

Looking at the results without control, it can be observed that as the load arrives to the middle of the prototype (after approximately 6 seconds), the deflection at midspan increases to a maximum value of 12.5 mm. This result, as expected, is around twice the value obtained for the equivalent scenario when only one pedestrian was crossing the footbridge.

The orange curves plot the results for the ON/OFF control test scenario. The maximum displacement (in absolute value) reaches a value of only 2.5 mm. This is lower than the value obtained for the test scenario with one pedestrian because a lower walking speed allows a better performance of the smart system. Again, comparing with the non-controlled scenario, deflections are reduced up to a fifth of the initial value.

As a third load scenario, the prototype was tested under the load of a unidirectional flow of pedestrians, to observe the behavior of the smart system in real service conditions of a footbridge. Pedestrians entered the prototype every 2-3 seconds, with an average of 2-3 pedestrians present on the footbridge simultaneously. To obtain a more realistic response, no specific restrictions on walking pace were given.

To evaluate the performance of the smart system when a pedestrian flow is crossing the footbridge, the midspan displacements over time are plotted in Figure 7.11. As in the previous analyses, the test scenarios included the structure without and with smart control.

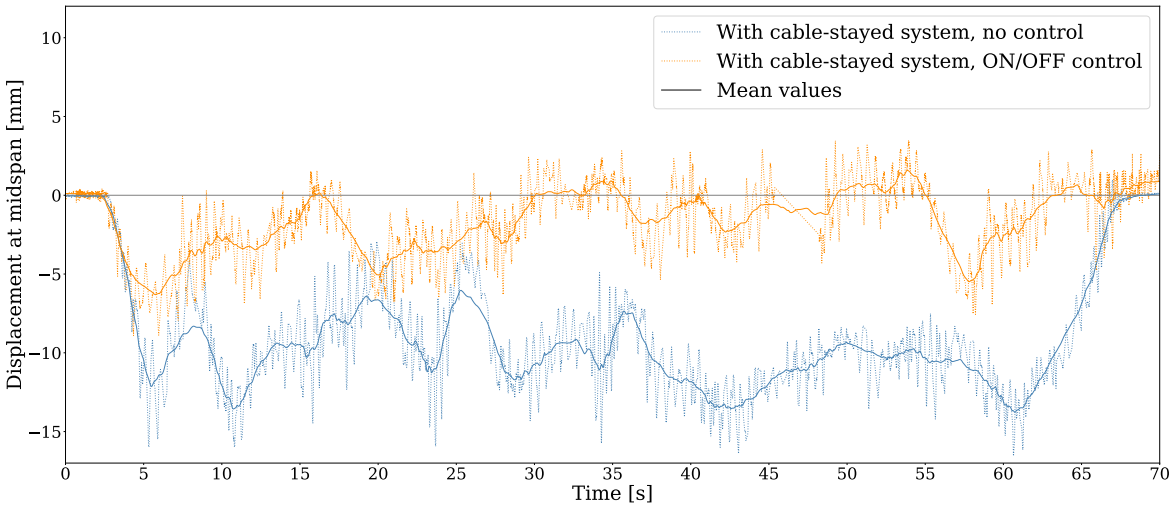

Figure 7.11: Experimental displacements at midspan vs. time, for an unrestricted flow of pedestrians.

The results clearly shed light on the effectiveness of the smart system, as the maximum deflection is successfully reduced from 13.5 mm (without control) to 6.0 mm (with control). Although the deflection reduction is lower with respect to the case with only two pedestrians (due to the worse performance of the smart system when subjected to uncontrolled live loads) the system still proves to be effective, achieving a deflection reduction of around 55%.

As a main finding, these results experimentally prove that deflections of the deck can be significantly reduced using a smart strategy. In addition, the performance of the system is affected by the speed of the load and the speed of the actuation. Finally, it should be noted that due to the delay of the response, the displacements exceed the thresholds, a fact that should be considered in the design process.

7.4 Dynamic behavior and vibration evaluation

7.4.1 Dynamic behavior

The second part of the experimental campaign focuses on the dynamic behavior of the prototype. This work was done in collaboration with professor J.M. Soria of the Universidad Politécnica de Madrid.

To provide a complete dynamic characterization, 10 piezoelectric accelerometers (ICP ® – PCB Piezotronics) with a sensitivity of 10 V/g were strategically placed, five on each side

of the structure. Data acquisition was conducted using a compactRIO 9067 data logger (National Instruments) equipped with three NI 9402 cards with 12 analog input channels. Dynamic experimental measurements were performed within the LabVIEW environment. A frequency sampling rate of 1000 Hz per channel and recordings of 300 seconds were chosen to effectively identify the modal parameters of the structure and eliminate the possibility of aliasing problems during post-processing of the ambient measurement. The signal is filtered by a low-pass Butterworth filter of order 4 with a cutoff frequency of 15 Hz. A decimation factor of 30 is applied obtaining a Nyquist frequency of 16.67 Hz. Figure 7.12 shows the ambient response in the time domain of the 10 channels, filtered and decimated.

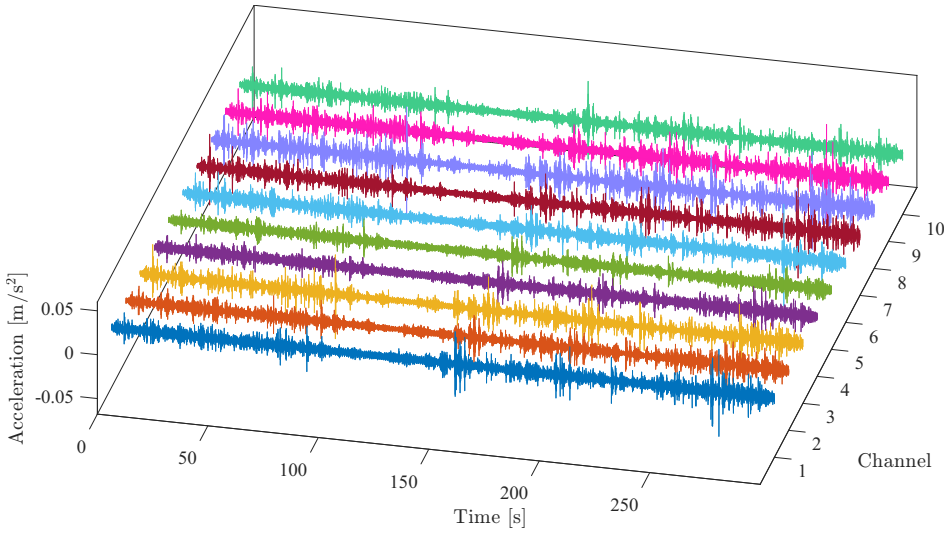

Figure 7.12: Ambient response in the time domain of the 10 channels.

In this study, the modal parameters of different vibration modes (eigenfrequencies, mode shapes and damping ratios) are obtained from ambient measurements. This is done using a covariance-driven stochastic subspace identification technique of operational modal analysis [84]. The method consists in selecting the average values of the modal parameters for each column of stable aligned poles of the stabilization diagram with a minimum number of stable poles [85]. This approach was chosen due to its ability to identify the underlying structural dynamics by exploiting the covariance structure of the measured data. This was achieved by programming it in MATLAB.

The modal parameters of the structure without any applied load are studied for four different scenarios:

- Scenario 0: prototype without cable-stayed system.
- Scenario 1: prototype with cable-stayed system, partially compensating the permanent

load ($\rho < 1$, the downward displacement at midspan due to the permanent load reaches 3 cm).

- Scenario 2: prototype with cable-stayed system, fully compensating the permanent load ($\rho = 1$, the displacement at midspan due to the permanent load is zero).
- Scenario 3: prototype with cable-stayed system, overcompensating the permanent load ($\rho > 1$, the upward displacement at midspan due to the permanent load reaches 2 cm).

The different values of the displacement at midspan are achieved by elongating or contracting the actuator. Consequently, the geometrical configuration of the structure for the three aforementioned scenarios is different, as there is a change of the rise. As indicated in the previous Section 7.3, a different value of f modifies the live load distribution between the cable-stayed system and the deck.

Figure 7.13 shows the frequency spectra obtained with the accelerometers situated at a quarter span (4.5 meters from the left support), obtained considering 8 blocks and an overlap of 50%. Also, the modal shapes for the different scenarios are depicted. The comparison of the different scenarios in the frequency domain spectra is possible because the ambient measurements were collected in a highly-controlled environment with consistent duration and excitation.

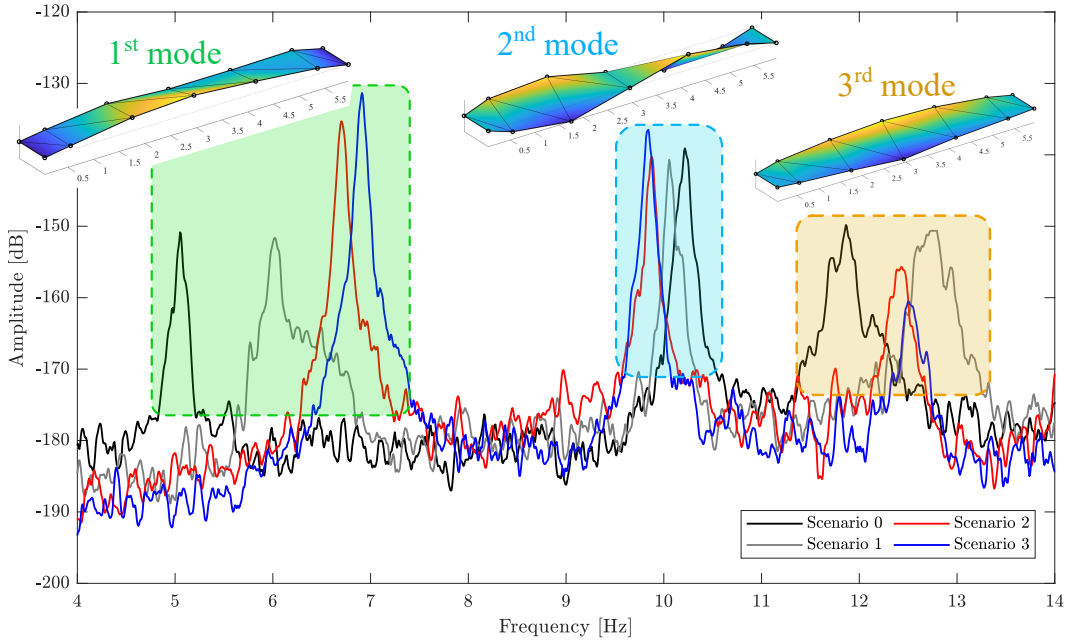

Figure 7.13: Frequency spectra obtained for the different scenarios and the modal shapes of the associated vibration modes.

Three vibration modes are observed between 0 and 14 Hz: one bending (first) and two torsional modes (second and third). The dynamic response of the structure is dominated by the first vibration mode, whose eigenfrequency is between 5.05 and 6.90 Hz, depending on the scenario. The introduction of a cable-stayed system strongly affects this bending mode as the stiffness of the structure increases. Also, the natural frequencies of the structure are influenced by the deviation force introduced by the midspan strut (the actuator in this case). Increasing this force leads to a reduction in the modal mass associated with the vibration mode, which subsequently increases the vibration frequency. However, it is noted that the axial compressive force in the deck, which arises from force equilibrium, has no effect on the vibration modes.

Table 7.1 summarizes the estimated values of the frequencies (represented in Figure 7.13) and damping ratios of the first three vibration modes for the different scenarios. As Soria et al. concluded [84], the damping estimation is highly dependent on the time window selected, and it has greater uncertainty than the estimated frequency values. For this reason, the analysis herein presented is focused on the variation of the frequency. However, some remarks can be made regarding the damping ratio: i) the torsional modes (second and third vibration modes) show a lower damping than the bending mode, and ii) the effect of adding a cable-stayed system has a major influence in the bending mode.

Table 7.1 Frequencies, f_i [Hz], and damping ratios, ζ_i [%], of the first three vibration modes for the different scenarios.

Scenario	f_1 [Hz]	f_2 [Hz]	f_3 [Hz]	ζ_1 [%]	ζ_2 [%]	ζ_3 [%]
0	5.05	10.22	11.85	0.78	0.75	0.71
1	6.04	10.07	12.65	1.15	0.70	1.01
2	6.71	9.86	12.43	1.16	0.72	0.97
3	6.95	9.83	12.50	1.27	0.72	0.79

7.4.2 Evaluation of vibrations caused by a single walking pedestrian

This section analyzes the dynamic performance of the prototype in the four previous scenarios in terms of accelerations and vibrations. Additionally, scenarios 2 and 3 are repeated activating the smart system with an ON/OFF actuator control law. As shown in Section 7.3.5, in this structure the static deflection prevails over the dynamic one. For this reason, the ON/OFF control law has been designed to correct the static deflection. The same philosophy could be applied to specifically improve the dynamic behavior, although this topic is out of

the scope of this thesis and it is addressed as a future line of research.

The experimental results shown in Figure 7.13 proved that the natural frequencies change depending on the rise of the cable-stayed system. Additionally, in extremely slender structures, such as this prototype, the pedestrian mass also alters the frequencies. Therefore, to allow a comparison among the different scenarios, instead of testing the footbridge at the natural frequency for each case, all tests have been performed at the same pedestrian walking pace. Specifically, a typical walking frequency of 1.87 Hz has been chosen [86], [87], corresponding to an approximate walking speed of 1 m/s (same as in the tests shown in Figure 7.9).

The Running Root Mean Square (RMS) acceleration is computed using τ-second time interval and it is defined as:

$$a_{\mathrm{RMS},\tau}(t) = \sqrt{\frac{1}{\tau}\int_{t-\tau}^{t} a^2(\tau)\ d\tau} \qquad [\,\mathrm{m/s^2}], \tag{7.2}$$

where τ is the integration time for running averaging (normally $\tau = 1\,\mathrm{s}$ is recommended) and t is the time of observation (instantaneous time). The maximum value of $a_{\mathrm{RMS}}(t)$ is usually referred to as the Maximum Transient Vibration Value (MTVV):

$$\mathrm{MTVV} = \max\left(a_{\mathrm{RMS},1}(t)\right), \quad t \in [0, T], \tag{7.3}$$

in which T is the duration of the measurement. This value is commonly used to asses the vibration serviceability of structures under human loading [88], [89]. Although comfort is not evaluated, the MTVV allows to avoid considering local peaks of the recorded data.

Aided by a metronome, a pedestrian performs a complete walk on the structure in each scenario to assess the level of acceleration experienced by the structure. Figure 7.14 shows the time history response acceleration at midspan for the structure without the cable-stayed system (scenario 0) for the pedestrian walking in both directions. In this specific scenario, a MTVV of 2.25 $\mathrm{m/s^2}$ is obtained.

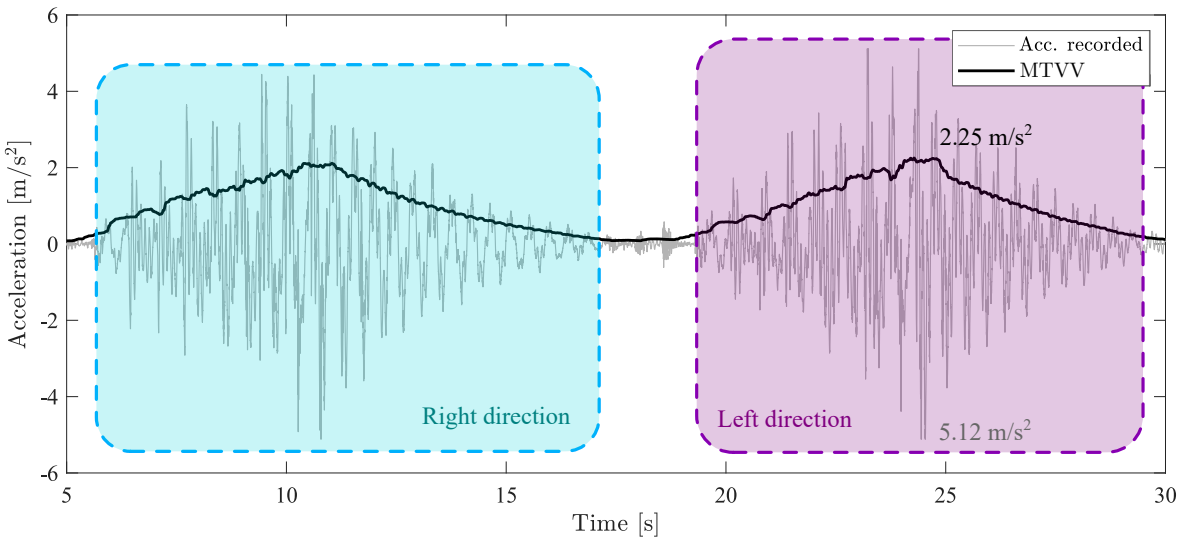

Figure 7.14: Time history response acceleration at midspan for pedestrian walking in both directions in scenario 0.

Following the same approach, the MTVV values for the remaining scenarios are obtained. Figure 7.15 summarizes these results, along with the vibration reduction (MTVV of each scenario compared to MTVV of scenario 0).

Installing the cable-stayed system (scenarios 1, 2 and 3) allows to reduce the MTVV value an average of 15.4%. When the smart control is used, the MTVV is reduced by 20.6% for scenario 2 and 12.6% for scenario 3. Overall, comparing to scenario 0, the higher vibration reduction is obtained when the active control is combined with a higher rise (scenario 3), where the initial prestress force overcompensates the permanent loads ($\rho > 1$).

It is interesting to observe that the MTVV values for scenarios 2 and 3 are very different when tested without control. However, when the smart system is activated, this difference is much smaller. This is because in the first case, the stiffness of the structure depends on its geometry (the rise for scenario 3 is higher than scenario 2), but when the control is activated, the load distribution between the deck and the cable-smart system is deliberately modified in order to increase the participation of the latter in bearing the loads.

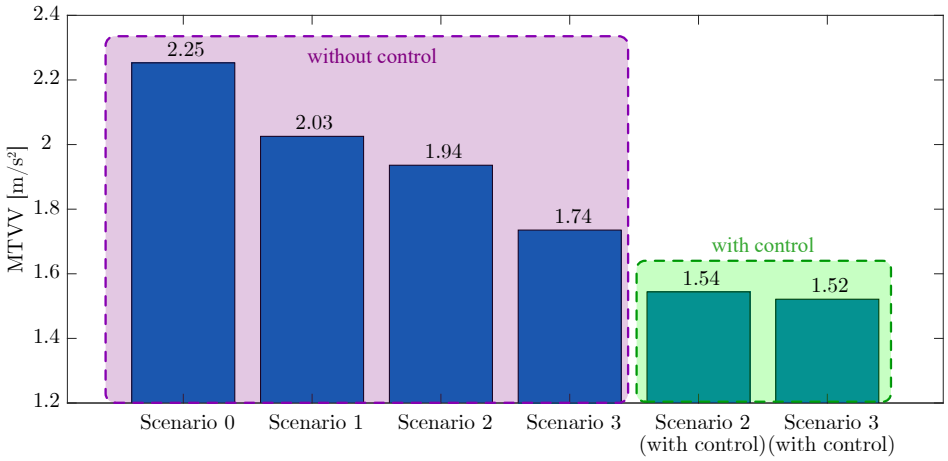

(a) MTVV.

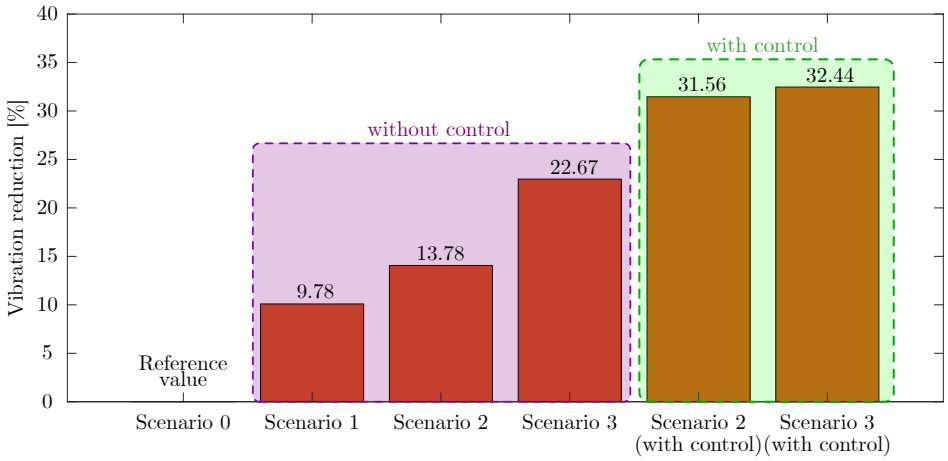

(b) Vibration reduction.

Figure 7.15: Vibration assessment of structural dynamic behavior of the prototype.

7.4.3 Evaluation of vibrations caused by a flow of pedestrians

This section analyses the dynamic performance of the prototype when subjected to an unrestricted pedestrian flow. Two tests are presented: with the structure working as a conventional cable-stayed footbridge (without control) and with the smart system activated (with control). The tests presented in this section are performed for scenario 3 (as described in Section 7.4.1), where the cable-stayed system is overcompensating the permanent load.

Unrestricted pedestrian traffic refers to a situation where there are many pedestrians walking on the footbridge simultaneously. Due to the stochastic nature of pedestrian flow, it should be studied probabilistically, considering several sources of randomness among the

pedestrian arrivals, step frequencies and velocities, force amplitudes and pedestrian weights. In the tests herein presented, 200-second measurements have been chosen to ensure repeated characteristics of the pedestrian flow, which will allow an accurate comparison between the two tests. To achieve a realistic response, no specific restrictions were given to the walking pace.

As explained in Section 7.3.5, a unidirectional pedestrian traffic flow is maintained with one pedestrian entering the prototype every 2-3 seconds, resulting in a pedestrian density between 0.48 and 0.71 pedestrians/m^2. According to the HIVOSS guideline [79], this corresponds to a dense or very dense pedestrian flow.

To study the dynamic behavior of the footbridge when subjected to this pedestrian flow, the Vibration Dose Value (VDV) is used. The VDV is a performance indicator that measures the cumulative effect of vibrations and quantifies the amount of vibration over a period of time. It takes into account the frequency, duration, and intensity of the vibration. It is computed as follows:

$$\mathrm{VDV} = \left[\int_0^T a^4(t)\,dt\right]^{0.25} \qquad \left[\mathrm{m/s^{1.75}}\right] \tag{7.4}$$

In Figures 7.16a and 7.16b, the time history acceleration at midspan is plotted against the time for both tests (with and without the smart system). Additionally, the VDV is also represented for each case.

Based on the comparison between the conventional and the smart structure, it is possible to reduce a 21.6% the measured MTVV: from 2.18 m/s^2 in the pedestrian traffic test without control, to 1.71 m/s^2 when the control system is activated. On the other hand, considering the cumulative nature of vibration, the final value of the VDV is reduced from 5.96 $m/s^{1.75}$ to 5.01 $m/s^{1.75}$, a reduction of 15.9%. This result demonstrates the improvement in vibrations achieved in the footbridge when using a smart system.

It is noted that the amplitude of the vertical acceleration caused by the pedestrian flow are of the same order of magnitude as those caused by a single pedestrian walking. This is because the vertical load of multiple pedestrians is distributed over a larger surface area, resulting in a lower dynamic amplification [90].

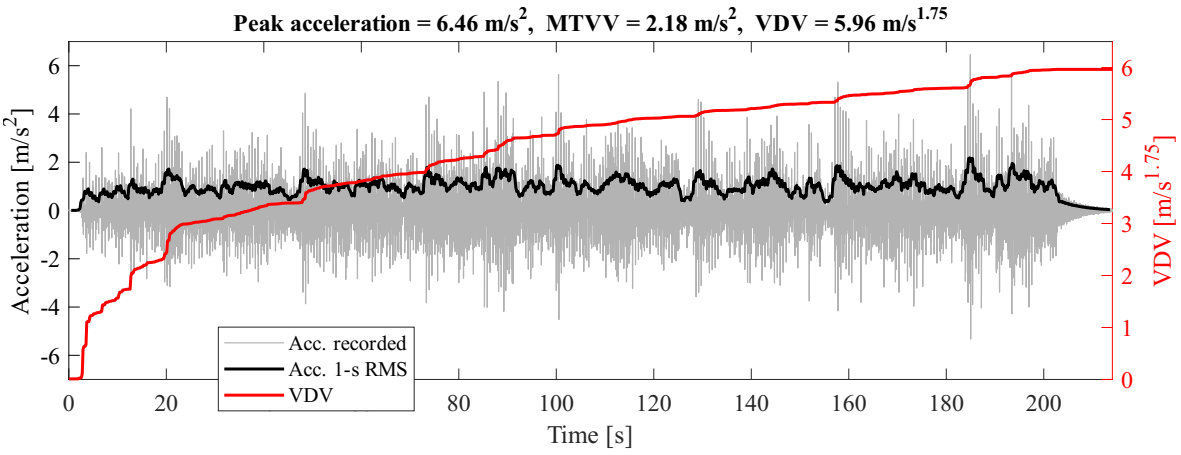

(a) Test without control (conventional structure).

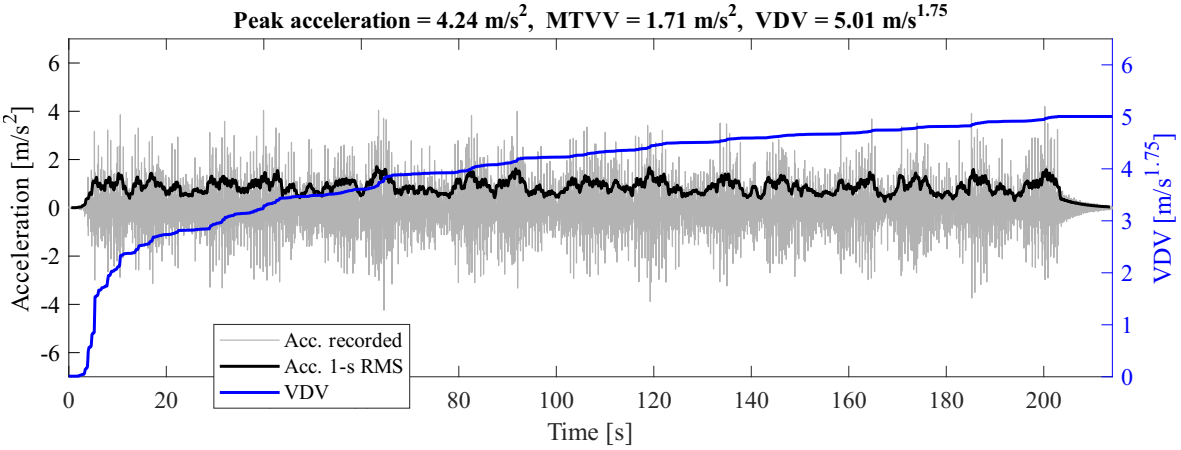

(b) Test with ON/OFF control (smart structure).

Figure 7.16: Time history acceleration at midspan under unrestricted pedestrian flow.

7.5 Conclusions

This chapter provided a physical demonstration of smart under-deck cable-stayed footbridges by illustrating the design, construction, and testing of a 6-meter-span prototype. The main findings of this section are:

- The experimental response under static loads is perfectly coherent with the expected behavior according to analytical and numerical models. In fact, differences between results oscillate in a range of 4-8%, which validates the accuracy of the theoretical models and demonstrates that the prototype is capable of performing well under static conditions.

- Both experimental and theoretical studies have determined the efficiency of the under-deck cable-stayed system. This efficiency is expressed by the factor ξ, which represents the portion of the live load resisted by the cables. A factor $\xi = 0.81$ has been obtained, indicating the significant contribution of the cable-stayed system in resisting live loads.

- The experimental results prove that the structural response under live load does not depend on the initial configuration of the system (permanent load and initial prestressing). In contrast, a variation of the geometry (e.g. a change of the rise) affects the live load distribution between the deck and the under-deck cable-stayed system. Furthermore, if the elongation of the actuator is significant, non-linear effects cannot be neglected.

- Under quasi-static loads (i.e., pedestrians slowly crossing the prototype) the contribution of the smart system depends on several variables, such as the magnitude and the speed of the load. In fact, in specific conditions (two people crossing the footbridge) the smart system allows reducing the maximum deflection up to a 80% of that obtained without control (from 12.5 mm to 2.5 mm).

- Under more realistic conditions, where the prototype is subjected to a flow of pedestrians walking at random paces, implementing the smart system results in a significant reduction of up to 55% in the maximum deflection.

- An experimental dynamic analysis demonstrates that the increase of stiffness achieved in the structure thanks to the cable-stayed system, raises the frequency of the first bending mode. Specifically, it increases from a frequency of 5.05 Hz without the cable-stayed system (scenario 0), to 6.90 Hz when the permanent loads are overcompensated by the cable-stayed system (scenario 3).

- The use of a cable-stayed system positively affects the dynamic response of the footbridge under live loads. Specifically, a mean reduction of 15.4% of the MTVV is obtained with the addition of the conventional cable-stayed system.

- The activation of the smart system with a simple ON/OFF control strategy allows to improve the pedestrian comfort because of the real-time modification of the structural geometry. The MTVV is reduced by a 12.6-20.6% (depending on the initial configuration of the structure) with respect to the equivalent scenarios without control and under a single pedestrian walking. In contrast, a 21.6% MTVV reduction is obtained under unrestricted pedestrian flow (VDV reduction of 15.9%).

The construction of experimental proofs-of-concept is essential to investigate the real response of innovative structural typologies like the one herein presented, where smart systems are integrated into the structure. Although the results previously presented show that relevant improvements can be achieved when using a smart system, as will be discussed in the section on future research (Section 9.2), there are several aspects that require further investigation before being able to successfully extrapolate this technology to real-scale demonstrators.